

Reformulating Parallel-Connected Lithium-Ion Battery Pack Dynamics with Interconnection Resistances as Ordinary Differential Equations

Jaffar Ali Lone, Nilsu Atlan, Simone Fasolato, Davide M Raimondo and Ross Drummond

Abstract—This work presents analytical solutions for the current distribution in lithium-ion battery packs composed of cells connected in parallel, explicitly accounting for the presence of interconnection resistances. These solutions enable the reformulation of the differential-algebraic equations describing the pack dynamics into a set of ordinary differential equations, thereby simplifying simulation and analysis. Conditions under which uniform current sharing across all cells occurs are also derived. The proposed formulation is validated against experimental data and confirms its ability to capture the key behaviours induced by interconnection resistances. These results can support the improved design and control of parallel-connected battery packs.

Index Terms—Parallel connected battery packs, Current distribution, Contact resistances, Analytical solution, Ordinary differential equations.

I. INTRODUCTION

TODAY, typical lithium-ion batteries have cell-level energy densities of roughly $\approx 100 - 500 \text{ Wh kg}^{-1}$ [1], significantly lower than those demanded by intensive applications such as electric aircraft and grid storage. For those applications, large battery packs formed by connecting several thousand individual cells in series and parallel are needed. Examples can be found in electric vehicles (such as the 7,104 cell pack of the Tesla Model S) and grid storage (such as the 18,900 cells used in [2] and the 50,000 cells used in [3]). The move towards large packs in recent years has shifted the focus of modeling and analysis away from lumping all individual cells together and treating them uniformly, towards recognizing the pack as a complex system in which each unique cell contributes to the overall dynamics. This perspective is essential because battery designs that perform well at the cell level may not necessarily retain those advantages at the pack-level. This was highlighted by Frith et al. [1] in their discussion of a *graphite-SiO_x*||NCA cell with an energy density of $\approx 250 \text{ Wh kg}^{-1}$ which dropped to $\approx 140 \text{ Wh kg}^{-1}$

Jaffar Ali Lone thanks the Ministry of Education, Govt. of India, for providing financial support via PMRF Grant no. 2701805.

Jaffar Ali Lone is with the Department of Electrical Engineering, Indian Institute of Technology Patna, India. jaffar_2121ee06@iitp.ac.in

Nilsu Atlan and Ross Drummond are with the School of Electrical and Electronic Engineering, University of Sheffield, UK.
ross.drummond@sheffield.ac.uk

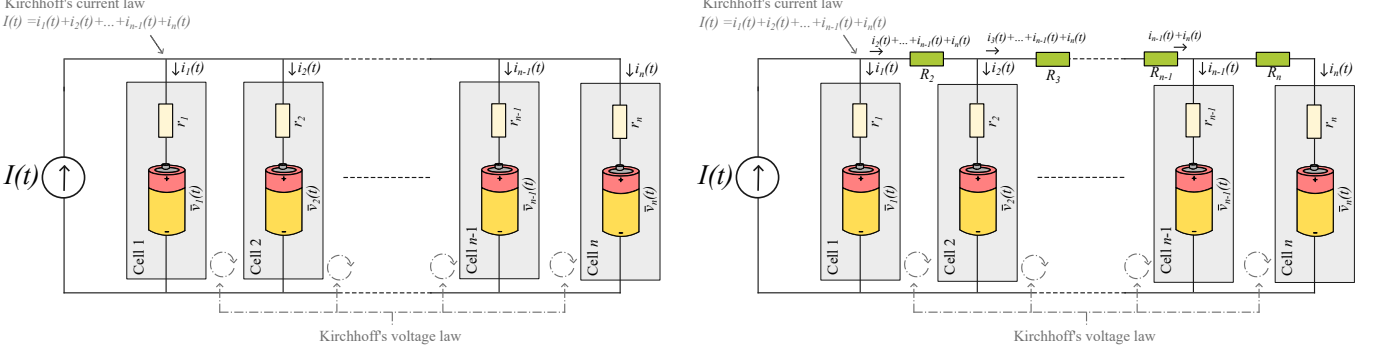
Simone Fasolato is with the Department of Electrical, Computer and Biomedical Engineering University of Pavia, IT.
simone.fasolato01@universitadipavia.it

Davide Raimondo is with the Department of Engineering and Architecture, University of Trieste, Trieste, IT.
davide.raimondo@univp.it

kg^{-1} at the pack-level. In contrast, a *graphite||LFP* cell with a significantly lower energy density of $\approx 180 \text{ Wh kg}^{-1}$ had a comparable pack-level energy density of $\approx 120 \text{ Wh kg}^{-1}$. In other words, higher cell-level energy densities do not necessarily lead to substantial performance gains at the pack-level. A range of factors contribute to this energy density gap, including the enhanced thermal and electrochemical stability of LFP cathodes which reduces the need for active cooling. As pack sizes increase, additional challenges emerge that contribute to reduced efficiency [1] and accelerate degradation [4]–[6]. These include state-of-charge [7] and temperature [5], [8] heterogeneities, as well as scalability issues in designing battery management system algorithms [9], [10].

Mathematical modeling can be used to reduce the performance drop-off between lithium-ion cells and packs, by offering deeper insight into pack-level behavior. In recent years, cell-level lithium-ion battery modelling has advanced rapidly, with a wide variety of codes now available including the electrochemical models of PyBaMM [11], LIONSIMBA [12], TOOFAB [13], and PETLION [14]. However, these benchmark codes currently do not scale effectively to the pack-level, especially in the case of parallel connections. Existing methods, such as Liionpack [15], have limitations including having to numerically solve the differential algebraic equations of Kirchhoff's laws at every time instant; as opposed to simply propagating the solution of an ordinary differential equation forward in time. The popularity of these codes highlights the need to extend recent advances in cell-level modelling to the pack-level, and so accelerate the development of open-source pack-level codes with comparable user-friendliness and simulation speeds.

To accurately model battery packs, the effects of connecting cells in series and in parallel must be taken into account. Series connections increase the pack voltage and thus contribute to higher power output, while parallel connections increase the overall capacity, enhance fault tolerance to open-circuit failures, and may enable partial self-balancing under certain conditions. Modelling cells in series is relatively straightforward as each cell receives the same current, allowing for the decoupling of their dynamics (although cells in series can still be thermally coupled together). Modelling cells in parallel is more complex since algebraic equations must be solved at each time step to determine the branch current distribution (i.e., the current flowing into each parallel branch—see Figure 1 for an illustration) to ensure that Kirchhoff's current and voltage laws are satisfied (see Equations (6) and (13) and also [16]–[18]).



(a) A parallel-connected lithium-ion battery pack *without* interconnection resistances.

Fig. 1. Two parallel-connected battery packs: (a) ideal case without interconnection resistances R_k , and (b) with R_k accounting for wire and interconnection resistances. The study examines how branch currents $i_k(t)$ distribute in response to these resistances.

These algebraic equations result in parallel pack models being described by *differential-algebraic equations* (DAEs) rather than *ordinary differential equations* (ODEs).

Solving DAEs is, in general, more computationally demanding than solving ODEs—a challenge that has motivated studies on tailored numerical methods [19]. For example, in [20], the authors proposed a method to improve the scalability of electrochemical model simulations for large battery packs composed of parallel-connected cells governed by DAEs. The approach leverages the Waveform Relaxation technique to decompose the system into smaller, more computationally efficient sub-problems, which are solved iteratively until convergence. While effective, the method yielded significant reductions in computation time only when a sufficiently large number of cells were connected in parallel.

The inherent complexity of DAE-based formulations has motivated the development of methods that first convert the DAEs into ODEs by solving the algebraic equations. For packs composed of parallel-connected cells, this requires solving Kirchhoff's laws to express the distribution of branch currents in terms of the model states and the applied current. Kirchhoff's laws can be solved either numerically or analytically. The *numerical* approach typically involves inverting a matrix—referred to in this paper as the A_{22} matrix, as defined in Eqn. (7) and in works such as [3], [17], [18]. Beyond the computational burden of performing matrix inversion at each time step, this approach often lacks the physical insight needed for pack-level design optimization. In contrast, *analytical* solutions avoid repeated matrix inversion—which can scale in complexity as $\mathcal{O}(n^3)$ where n is the matrix dimension [21]—and reveal how branch currents redistribute throughout the pack. These insights can support better pack design decisions, reduce degradation gradients [4], [5], [22], [23], minimize current and parameter heterogeneity [24]–[27], and improve algorithms for pack-level battery management systems [7].

Existing analytical solutions for current distributions in battery pack models include those presented in [28], [29], as well as earlier studies such as [30], which focused on cell models with linear open-circuit voltage curves, and [31],

which neglected state-of-charge dynamics. A key limitation of these prior solutions is that they did not account for the interconnection resistances between cells, such as those arising from bus bars or wiring. In many practical applications, interconnection resistances can exceed the internal resistances of the cells themselves, leading to significant heterogeneity across the pack. This point was emphasized by Piombo et al. [32], who stated that:

“According to the results, the interconnection resistance is the most relevant contributor to heterogeneous performance within the (parallel) string.”

However, existing analytical modelling approaches have not been generalized to battery packs with interconnection resistances. Instead, alternative methods, such as the one proposed by [2], have been adopted. In that paper, rather than directly enforcing the algebraic equations of Kirchhoff's laws in the parallel pack model equations, a control theory approach was adopted with a proportional-integral controller regulating the currents amongst the parallel-connected cells (based on voltage differentials relative to the mean voltage of all cells) to drive the error in the voltage constraints to zero. Although this approach enables dynamic current balancing, it lacks closed-form expressions for the branch currents and relies on appropriate tuning of control parameters to ensure stability.

This paper addresses this gap by generalizing explicit solutions for branch currents to account for interconnection resistances in the pack (see Section IV).

Contributions: The main contributions of this paper are:

- 1) Derivation of analytical expressions for branch current distributions in battery packs composed of parallel-connected cells, as functions of the model states and the applied current, both with and without interconnection resistances.
- 2) Application of these analytical expressions to transform the DAE-based pack model into an ODE formulation. This reformulation offers computational advantages and provides deeper insight into current distributions across the pack.
- 3) Experimental validation of the proposed analytical solution using measured data. Simulations also illustrate the

emergence of current fluctuations within the pack.

- 4) Identification of pack configurations with interconnection resistances that enable uniform cell responses. In particular, generalized QR-matching conditions are derived for packs with interconnection resistances.

To the best of the authors' knowledge, this is the first derivation of analytical current distributions for parallel-connected battery packs that account for interconnection resistances. The theoretical results are validated against experimental data and simulations of packs considering both $\text{LiNi}_x\text{Mn}_y\text{Co}_{1-x-y}\text{O}_2$ (NMC) and LiFePO_4 (LFP) cells. Code to run the models used in this paper can be found at <https://github.com/jaffarlon07/Parallel-Pack-Paper-MATLAB-Code.git>.

II. MODELING PACKS OF PARALLEL-CONNECTED CELLS

We consider the problem of modeling battery packs composed of parallel-connected cells, as illustrated in Figures 1a and 1b. For simplicity, we use the term *pack* to refer to any collection of connected cells. This simplified use of the term pack is intended to streamline the language of the paper, although we acknowledge that, in practice, packs are often assembled from smaller groupings of cells—such as modules—and this terminology may introduce some ambiguity.

A. Dynamics of a single cell

The dynamics of each cell in the pack, denoted as $h_k(x_k(t), i_k(t)) : \mathbb{R}^m \times \mathbb{R} \rightarrow \mathbb{R}^m$ are described by

$$\frac{d}{dt}x_k(t) = h_k(x_k(t), i_k(t)), \quad \forall k = 1, 2, \dots, n, \quad (1a)$$

where $x_k \in \mathbb{R}^m$ is the state of the k^{th} cell in the parallel pack and $i_k(t) \in \mathbb{R}$ denotes the branch current it receives. The voltage of cell k , $v_k(t) \in \mathbb{R}$, is assumed to include a resistance term

$$v_k(t) = \bar{v}(x_k(t)) + r_k i_k(t) \quad \forall k = 1, 2, \dots, n. \quad (1b)$$

Here, $\bar{v}(x_k(t))$ represents the state-dependent component of cell k 's voltage, incorporating effects such as the open-circuit voltage, while r_k represents its series resistance. As illustrated in Figure 1, the individual cell models are interconnected, with R_k representing the interconnection resistance between them. A key assumption in this work is that the Ohmic drop, $r_k i_k(t)$, is a linear function of the current. This linearity is fundamental, as it enables the branch currents $i_k(t)$ to be computed using linear algebra. While some battery models include nonlinear resistances, such as the \sinh^{-1} term arising from the homogenization of Butler-Volmer kinetics in single-particle models [33], many widely used models assume linear resistances, including most equivalent circuit models [34] and the Doyle-Fuller-Newman model [35], [36]. Furthermore, because current fluctuations in uniform packs are typically small [37] and the dynamics remain stable [38], linearising the nonlinear resistances often yields sufficiently accurate approximations. In contrast, the nonlinearity of the state-dependent voltage component $\bar{v}(x_k(t))$ —such as the open-circuit voltage—does not impact the analysis.

The cell-level model structure in Eqn. (1) is intentionally kept general to emphasize the broad applicability of the analytical solutions for branch currents $i_k(t)$ developed in Sections III-B and IV-C. This modeling framework encompasses a wide range of battery models, including equivalent circuit models with thermal dynamics, as well as certain classes of electrochemical models, such as the Doyle–Fuller–Newman electrochemical model [28], [35], [36], [39].

B. Dynamics of battery packs with parallel-connected cells

This paper investigates the behaviour of n parallel-connected cell models from Eqn. (1), as illustrated in Fig. 1. Two parallel configurations are considered:

- One that includes interconnection resistances (Section IV and Figure 1b).
- Another that neglects them (Section III and Figure 1a).

The configuration including interconnection resistances (Fig. 1b) follows the setup in [2], while the other without resistances (Fig. 1a) mirrors [28]. Specifically, [28] models n parallel-connected cells without interconnection resistances (i.e., resistances between cell bus bars), whereas [2] accounts for wiring resistances commonly found in practical setups [2], [37]. These resistances, denoted as R_k , play a crucial role in shaping current distributions [32], as they reduce the amount of current reaching cells located further along the electrical path within the pack.

For both pack configurations, the objective is to derive analytical expressions for the current distribution $i_k(t)$ flowing into each cell in terms of the model states and the applied current $I(t)$. To proceed, we define the pack's state vector and the vector of branch currents i_k entering each cell as follows

$$x(t) = \begin{bmatrix} x_1(t) \\ x_2(t) \\ \vdots \\ x_n(t) \end{bmatrix}, \quad i(t) = \begin{bmatrix} i_1(t) \\ i_2(t) \\ \vdots \\ i_n(t) \end{bmatrix}.$$

The vector of cell currents $i(t)$ arises from the distribution of the applied current $I(t)$ among the parallel-connected cells, in accordance with Kirchhoff's current law.

III. PARALLEL CELLS WITHOUT INTERCONNECTION RESISTANCES

Consider a battery pack composed of parallel-connected cells with no interconnection resistances. In this idealized scenario, the cells are assumed to be perfectly connected to bus bars, which are modeled as having zero resistance. This setup, illustrated in Fig. 1a, has been extensively studied in previous works, such as [28] and later in [29], but is included here to complete the analysis and highlight the difficulty in generalising to packs with interconnection resistances.

A. Kirchhoff's laws with $R_k = 0$

For the parallel pack of Fig. 1a without interconnection resistances, Kirchhoff's voltage law requires that the voltages of all individual cells in the pack are equal, i.e.

$$v_j(t) = v_k(t), \quad \text{for all } k, j = 1, \dots, n, \quad (2a)$$

or, alternatively,

$$\bar{v}_j(x_j(t)) + r_j i_j(t) = \bar{v}_k(x_k(t)) + r_k i_k(t), \quad \text{for all } k, j = 1, \dots, n. \quad (3a)$$

Since Eqn. (2a) holds for any j if it holds for one, we can set $j = 1$ in Eqn. (2) and express it in a more compact form

$$\bar{v}_1(x_1(t)) + r_1 i_1(t) = \bar{v}_k(x_k(t)) + r_k i_k(t), \quad \text{for all } k = 2, \dots, n. \quad (4a)$$

At the same time, Kirchhoff's current law requires that the branch currents, $i_k(t)$, sum to the applied current, $I(t)$, such that

$$\sum_{k=1}^n i_k(t) = I(t). \quad (4b)$$

The algebraic equations defining Kirchhoff's current law for the parallel pack in Fig. 1a can then be written in the matrix form

$$A_{22}i(t) = q(x(t)), \quad (5)$$

with

$$q(x(t)) = \begin{bmatrix} I(t) \\ \bar{v}_2(t) - \bar{v}_1(t) \\ \bar{v}_3(t) - \bar{v}_1(t) \\ \vdots \\ \bar{v}_n(t) - \bar{v}_1(t) \end{bmatrix}, \quad A_{22} = \begin{bmatrix} 1 & 1 & \dots & \dots & 1 \\ r_1 & -r_2 & 0 & \dots & 0 \\ r_1 & 0 & -r_3 & \ddots & \vdots \\ \vdots & \vdots & \ddots & \ddots & 0 \\ r_1 & 0 & \dots & 0 & -r_n \end{bmatrix}. \quad (6)$$

The branch currents could then be determined by inverting the A_{22} matrix

$$i(t) = A_{22}^{-1} q(x(t)). \quad (7)$$

By examining the structure of matrix A_{22} , and noting that $r_k \geq 0$, $\forall k = 1, \dots, n$, it follows that its columns are linearly independent either if $r_1 > 0$ or, in the case $r_1 = 0$, if and only if $r_k > 0$, for all $k = 2, \dots, n$. The following section shows how these branch currents could instead be computed analytically, without having to invert the A_{22} matrix, by simply solving Eqn. (5).

B. Distribution of branch currents with $R_k = 0$

Kirchhoff's voltage laws of Eqn. (4) can be expressed as

$$i_2(t) = \frac{1}{r_2}(r_1 i_1(t) - \Delta \bar{v}_{21}(t)), \quad (8a)$$

$$i_3(t) = \frac{1}{r_3}(r_1 i_1(t) - \Delta \bar{v}_{31}(t)), \quad (8b)$$

\vdots

$$i_n(t) = \frac{1}{r_n}(r_1 i_1(t) - \Delta \bar{v}_{n1}(t)), \quad (8c)$$

using the notation $\Delta \bar{v}_{jk}(t) = \bar{v}_j(t) - \bar{v}_k(t)$. Substituting these expressions into the current law of (4b) gives

$$\begin{aligned} I(t) &= i_1(t) + i_2(t) + \dots + i_n(t), \\ &= i_1(t) + \sum_{\ell=2}^n \frac{1}{r_\ell}(r_1 i_1(t) - \Delta \bar{v}_{\ell 1}(t)). \end{aligned} \quad (9)$$

The first branch current, $i_1(t)$, can then be expressed in terms of the model's state and the applied current $I(t)$ only

$$i_1(t) = \left(r_1 \sum_{\ell=1}^n \frac{1}{r_\ell} \right)^{-1} \left(\sum_{k=2}^n \frac{\Delta \bar{v}_{k1}(t)}{r_k} + I(t) \right). \quad (10a)$$

Using (10a), the currents of the other cells can be expressed as

$$i_j(t) = \frac{1}{r_j} \left(\left(\sum_{\ell=1}^n \frac{1}{r_\ell} \right)^{-1} \left(\sum_{k=2}^n \frac{\Delta \bar{v}_{k1}(t)}{r_k} + I(t) \right) - \Delta \bar{v}_{j1}(t) \right) \quad (10b)$$

for all $j = 2, 3, \dots, n$.

Therefore, in the absence of interconnection resistances, the currents of parallel-connected cells are defined by Eqn. (10). This means that there is no need to invert the A_{22} matrix of Eqn. (6). Substituting Eqns. (10) into the cell-level models in Eqn. (1) allows the parallel pack model to be reformulated as a set of ordinary differential equations, as the algebraic variables $i(t)$ become explicit functions of the differential states and the applied current.

IV. PARALLEL CELLS With INTERCONNECTION RESISTANCES

In practical settings, particularly in prototype designs, battery packs exhibit interconnection resistances between cells. The algebraic expression for the branch currents given in Equation (10a) is no longer valid in the presence of these resistances, as the additional ohmic drops influence the current distribution within the pack. This section addresses the issue by deriving an expression for the current distribution in the configuration shown in Figure 1b, explicitly accounting for interconnection resistances. To the best of the authors' knowledge, analytical expressions for current distributions in parallel-connected packs with interconnection resistances have not been previously reported and represent a central contribution of this work. Using the derived currents (see Eqn. (25)), the DAE model of the parallel pack can be reformulated as an ODE involving only the model parameters, state variables, and the applied pack current.

A. Kirchhoff's laws with $R_k \neq 0$

Consider the pack shown in [2, Fig. 4] and reproduced here in Fig. 1b. The difference between this pack and the one from [28] lies in the interconnection resistances R_k between the cells. In this case, Kirchhoff's current and voltage laws take the form

$$\sum_{k=1}^n i_k(t) = I(t), \quad (11a)$$

$$r_1 i_1(t) + \bar{v}_1(t) = R_2 \left(\sum_{k=2}^n i_k(t) \right) + r_2 i_2(t) + \bar{v}_2(t), \quad (11b)$$

$$r_2 i_2(t) + \bar{v}_2(t) = R_3 \left(\sum_{k=3}^n i_k(t) \right) + r_3 i_3(t) + \bar{v}_3(t), \quad (11c)$$

$$\vdots$$

$$r_{n-1} i_{n-1}(t) + \bar{v}_{n-1}(t) = R_n i_n(t) + r_n i_n(t) + \bar{v}_n(t). \quad (11d)$$

This system of equations can be written in a form analogous to Eqn. (6) with

$$A_{22}i(t) = q(x(t)) \quad (12)$$

and

$$A_{22} = \begin{bmatrix} 1 & 1 & \dots & \dots & 1 \\ r_1 & -(r_2 + R_2) & -R_2 & \dots & -R_2 \\ 0 & r_2 & -(r_3 + R_3) & \ddots & -R_3 \\ \vdots & \ddots & \ddots & \ddots & R_{n-1} \\ 0 & \dots & 0 & r_{n-1} & -(R_n + r_n) \end{bmatrix}. \quad (13)$$

B. Distribution of branch currents with $R_k \neq 0$

For the parallel pack shown in Fig. 1b, the objective of this section is to express the pack's branch currents, $i_k(t)$, in terms of its states, $x(t)$, and the applied current, $I(t)$. To achieve this, Kirchhoff's voltage laws, as outlined in (11b)-(11d), are first rewritten as

$$i_{n-1}(t) = \frac{1}{r_{n-1}} ((R_n + r_n)i_n(t) + \bar{v}_n(t) - \bar{v}_{n-1}(t)), \quad (14a)$$

$$i_{n-2}(t) = \frac{1}{r_{n-2}} \left((R_{n-1} + r_{n-1})i_{n-1}(t) + R_{n-1}i_n(t) + \bar{v}_{n-1}(t) - \bar{v}_{n-2}(t) \right), \quad (14b)$$

⋮

$$i_1(t) = \frac{1}{r_1} \left(r_2 i_2(t) + R_2 \sum_{k=2}^n i_k(t) + \bar{v}_2(t) - \bar{v}_1(t) \right). \quad (14c)$$

In contrast to Equation (10a), expressing the first branch current $i_1(t)$ in terms of the model states, via the voltages $\bar{v}_k(t)$ and the applied current $I(t)$, is no longer straightforward when interconnection resistances are present in the pack. To solve Eqn. (14) for the branch currents $i_k(t)$, we first introduce the variables $S_k(t)$, defined as the sum of the currents from branch k to n , as follows

$$S_k(t) = \sum_{j=k}^n i_j(t). \quad (15)$$

Additionally, Kirchhoff's current law implies the following relations

$$S_1(t) = \sum_{k=1}^n i_k(t) = I(t), \quad S_n(t) = i_n(t) \quad (16)$$

which will be used later in the analysis (see Eqn. (24)). Kirchhoff's laws can then be expressed in terms of the “current sum” variables $S_k(t)$. Before proceeding, we define the following variables

$$\theta_k = \frac{r_k}{r_{k-1}}, \quad \rho_k(t) = \frac{\bar{v}_k(t) - \bar{v}_{k-1}(t)}{r_{k-1}}, \quad \omega_k = \frac{R_k}{r_{k-1}}.$$

Kirchhoff's voltage laws (14) can then be expressed as

$$i_{n-1}(t) = \theta_n i_n(t) + \omega_n i_n(t) + \rho_n(t), \quad (17a)$$

$$i_{n-2}(t) = \theta_{n-1} i_{n-1}(t) + \omega_{n-1} (i_{n-1}(t) + i_n(t)) + \rho_{n-1}(t), \quad (17b)$$

$$i_{n-3}(t) = \theta_{n-2} i_{n-2}(t) + \omega_{n-2} \sum_{k=n-2}^n i_k(t) + \rho_{n-2}(t), \quad (17c)$$

⋮

$$i_2(t) = \theta_3 i_3(t) + \omega_3 \sum_{k=3}^n i_k(t) + \rho_3(t), \quad (17d)$$

$$i_1(t) = \theta_2 i_2(t) + \omega_2 \sum_{k=2}^n i_k(t) + \rho_2(t). \quad (17e)$$

Using the fact that

$$i_k(t) = S_k(t) - S_{k+1}(t), \quad \forall k = 1, \dots, n-1, \quad (18)$$

then Eqns. (17) can be expressed as

$$S_{n-1}(t) - S_n(t) = \theta_n S_n(t) + \omega_n S_n(t) + \rho_n(t), \quad (19a)$$

$$S_{n-2}(t) - S_{n-1}(t) = \theta_{n-1} (S_{n-1}(t) - S_n(t)) + \omega_{n-1} S_{n-1}(t) + \rho_{n-1}(t), \quad (19b)$$

$$S_{n-3}(t) - S_{n-2}(t) = \theta_{n-2} (S_{n-2}(t) - S_{n-1}(t)) + \omega_{n-2} S_{n-2}(t) + \rho_{n-2}(t), \quad (19c)$$

⋮

$$S_2(t) - S_3(t) = \theta_3 (S_3(t) - S_4(t)) + \omega_3 S_3(t) + \rho_3(t), \quad (19d)$$

$$S_1(t) - S_2(t) = \theta_2 (S_2(t) - S_3(t)) + \omega_2 S_2(t) + \rho_2(t). \quad (19e)$$

After defining the parameters $\alpha_k = (1 + \theta_k + \omega_k)$ for $k = 2, \dots, n$, then Eqns. (19) can be written more compactly as

$$S_{n-1}(t) = \alpha_n S_n(t) + \rho_n(t), \quad (20a)$$

$$S_{n-2}(t) = \alpha_{n-1} S_{n-1}(t) - \theta_{n-1} S_n(t) + \rho_{n-1}(t), \quad (20b)$$

$$S_{n-3}(t) = \alpha_{n-2} S_{n-2}(t) - \theta_{n-2} S_{n-1}(t) + \rho_{n-2}(t), \quad (20c)$$

$$\vdots \quad (20d)$$

$$S_2(t) = \alpha_3 S_3(t) - \theta_3 S_4(t) + \rho_3(t), \quad (20e)$$

$$S_1(t) = \alpha_2 S_2(t) - \theta_2 S_3(t) + \rho_2(t). \quad (20f)$$

C. Recurrence formulas for the branch currents

Next, define two sequences β_k and f_k which propagate backwards through the pack from $k = n+1$ to $k = 2$. Specifically, β_k is defined by the recursion

$$\beta_{n+1} = 1, \quad (21a)$$

$$\beta_n = \alpha_n, \quad (21b)$$

$$\beta_k = \alpha_k \beta_{k+1} - \theta_k \beta_{k+2}, \quad \forall k = 2, \dots, n-1, \quad (21c)$$

and f_k by

$$f_{n+1} = 0, \quad (22a)$$

$$f_n = \rho_n(t), \quad (22b)$$

$$f_k = \alpha_k f_{k+1} - \theta_k f_{k+2} + \rho_k(t) \quad \forall k = 2, \dots, n-1. \quad (22c)$$

Using these two sequences, Eqns. (20) can express $S_{k-1}(t)$ in terms of $S_n(t)$ via

$$S_{k-1}(t) = \beta_k S_n(t) + f_k, \quad k = 2, \dots, n. \quad (23)$$

This approach is similar to the one used in Eqn. (10a) without interconnection resistances. However, when interconnection resistances are taken into account, the solution is expressed in terms of the cascaded current sums, $S_k(t)$. Using the recursive definitions of f_k and β_k , as well as the relationship between

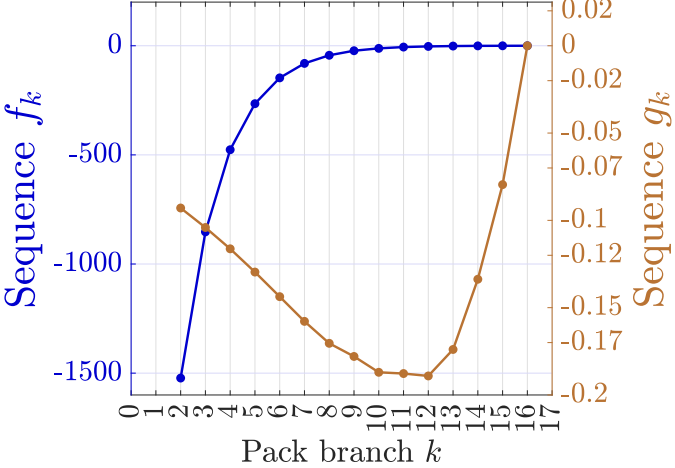


Fig. 2. Sequences f_k (navy blue) and g_k (orange) at the end of a discharge profile for a parallel-connected pack of $n = 15$ LFP cells with interconnection resistances and $c = 0.5$. The sequence f_k grows exponentially as k decreases from $n + 1$ to 2, while the scaled sequence g_k remains bounded, facilitating simulation and storage for large packs.

Kirchhoff's current law and $S_1(t)$ in (16), it is now possible to write

$$S_1(t) = \beta_2 S_n(t) + f_2 = I(t). \quad (24)$$

Solving Eqn. (24) for $S_n(t)$, and using the relation $S_n(t) = i_n(t)$ from (16), gives

$$S_n(t) = \frac{I(t) - f_2}{\beta_2} = i_n(t). \quad (25)$$

The final branch current, $i_n(t)$, has now been expressed in terms of the model's states, $x(t)$, and the applied current, $I(t)$. Once $i_n(t)$ is determined, the remaining currents $i_{1:n-1}(t)$ can be obtained by backward propagation through the pack via (17). In other words, substituting Eqn. (25) into (17) provides an explicit solution for the branch currents without requiring the inversion of the A_{22} matrix in Eqn. (13). This result implies an inverse of A_{22} exists as long as $\beta_2 \neq 0$, a condition defined by the sequence of Eqn. (21).

D. Comments

Section IV-B presented the derivation of the current distribution in the parallel pack of Fig. 1b, accounting for the interconnection resistances. Computing the branch currents requires first evaluating $i_n(t)$ using Eqn. (25), which is then used in Eqn. (17) to determine the remaining currents $i_k(t)$. The evaluation of $i_n(t)$ itself involves a backward recursion through the pack to compute the sequences β_k and f_k defined in Eqns. (21)–(22). Numerical experiments suggest that the recursion in Eqns. (21)–(22) can exhibit instability, potentially leading to numerical errors in large packs. By first focusing on f_k , a rough explanation for the instability could be inferred by thinking of Eqn. (21) as a time-varying discrete-time system running backwards in time from $k = n + 1$ to $k = 2$. The coefficients in this sequence satisfy $\alpha_k > 1$ and $\alpha_k > \theta_k$, conditions that imply the recursion is unstable. This instability is evident in Figure 2, which shows exponential growth in the

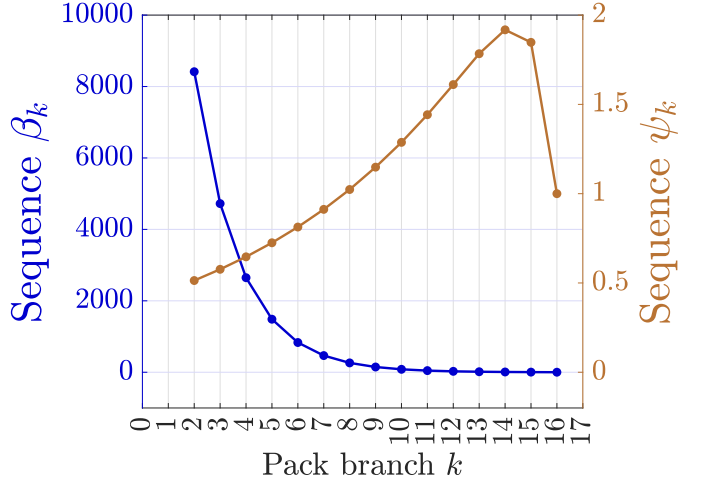


Fig. 3. Sequences β_k (navy blue) and ψ_k (orange) at the end of a discharge profile for a parallel-connected pack of $n = 15$ LFP cells with interconnection resistances and $c = 0.5$. Again, the sequences β_k grows exponentially as k decreases from $n + 1$ to 2, while the scaled sequence ψ_k remains bounded.

values of f_k , as k propagates backwards, for an $n = 15$ LFP pack. Even though the dynamics of (22) are finite-time, the instability could introduce problems when storing the sequence f_k when n is large, as the values approaching f_1 would grow rapidly, slow down the computations, and reduce the solution accuracy. To avoid storing these large numbers, it is proposed to define a new variable

$$g_k = c^{n+1-k} f_k, \quad (26)$$

which dynamically scales f_k by a scalar c . The dynamics for this scaled variable are

$$g_{n+1} = 0, \quad (27a)$$

$$g_n = c \rho_n(t), \quad (27b)$$

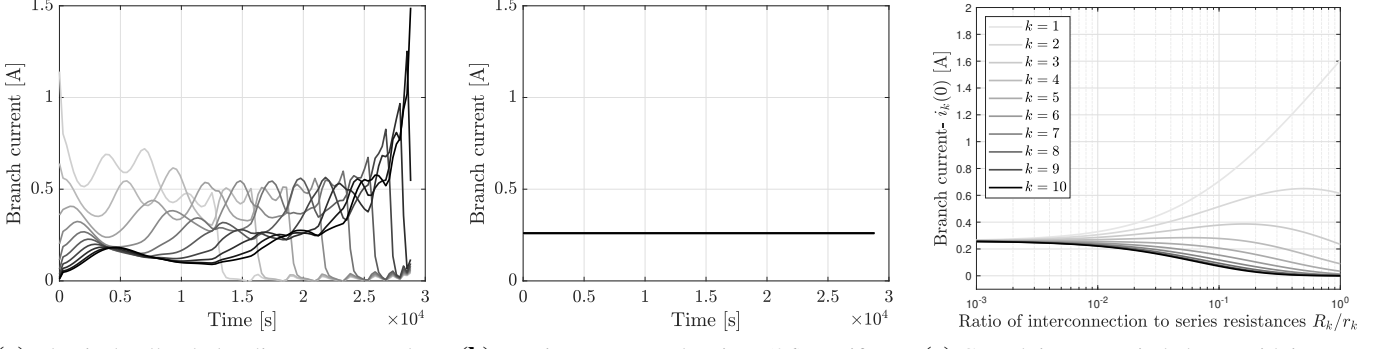
$$g_k = c \alpha_k g_{k+1} - c^2 \theta_k g_{k+2} + c^{n+1-k} \rho_k(t), \quad \forall k = 2, \dots, n-1. \quad (27c)$$

Selecting $0 < c < 1$ scales the dynamics, and, because all the dynamics are linear, it is then possible to recover f_k from g_k and so obtain the branch currents from (22). Computing the branch currents in this way using the bounded g_k sequence avoids the need to store the unstable variables f_k and allows the method to scale to large packs.

Figure 2 demonstrates how the scaled sequence g_k can reduce the effect of the instability in propagating through f_k . For this plot, $c = 0.5$ and the resulting g_k is both stable and bounded, whereas f_k grows exponentially as k propagates backwards through the pack.

The sequence β_k suffers from similar instability issues as f_k . A similar fix to Eqn. (26) can be found by defining a new variable

$$\psi_k = c^{n+1-k} \beta_k \quad (28)$$



(a) Identical cells: darker lines correspond to higher-indexed cells.

(b) Resistances tuned using (36): uniform current sharing achieved.

(c) Growth in current imbalance with increasing R_k/r_k .

Fig. 4. Current distributions during 1C charging for ten LFP cells connected in parallel using the parameter values from Section V. Subfigure (a) shows the case with identical cells, resulting in uneven current distribution. Subfigure (b) demonstrates how tuning R_k according to (36) leads to equal current sharing. Subfigure (c) illustrates the increase in current variation as the ratio R_k/r_k increases.

to transform the β_k dynamics from Eqn. (21) into

$$\psi_{n+1} = 1, \quad (29a)$$

$$\psi_n = c \alpha_n, \quad (29b)$$

$$\beta_k = c \alpha_k \psi_{k+1} - c^2 \theta_k \psi_{k+2}, \quad \forall k = 2, \dots, n-1. \quad (29c)$$

The original sequence β_k can then be obtained by inverting Eqn. (28). Figure 3 compares these two sequences for the pack setup of Figure 2. Again, it shows the instability of the original sequence, in this case β_k , and the convergent behaviour of the scaled one, ψ_k . As discussed above, this approach can enable the method to scale to large packs.

E. Uniform charging: Generalised QR-matching

Whilst the focus of the above analysis has been on determining how current heterogeneities form across a pack, the analytic current distributions of Eqn.s (10) and (17) can also be used to solve the reverse problem; how should the pack be designed such that all cells are used uniformly? For the case of two cells connected in parallel without interconnection resistances, this problem was solved by Weng et al. [22] with their proposed QR-matching conditions. In particular, they considered cells with dynamics for the state-of-charge, $z_k(t)$,

$$\dot{z}_k(t) = \frac{i_k(t)}{Q_k} = \ell_k(t), \quad (30)$$

with Q_k being the capacitances and ℓ_k the normalised charging rates for cell k . The QR-condition for uniform packs can be derived by noting that initially, $\Delta \bar{v}_{k1}(0) = 0$, and if all cells charge at the same rate then $\Delta \bar{v}_{k1}(t) = 0$. The problem can then be cast as finding conditions such that $\ell_k(t) = \ell_j(t)$ for all k and j . This is determined by rewriting the Kirchhoff voltage laws of Eqn. (4) as

$$0 = r_1 Q_1 \frac{i_1(t)}{Q_1} - r_k Q_k \frac{i_k(t)}{Q_k} = r_1 Q_1 \ell_1(t) - r_k Q_k \ell_k(t) \quad (31)$$

which implies a uniform pack is achieved with QR matching, as in

$$Q_1 r_1 = Q_k r_k. \quad (32)$$

The following generalises these conditions for uniform packs to the case when there are interconnection resistances. In this case, it is possible to again set $\Delta \bar{v}_{k1}(t) = 0$ and rewrite the voltage laws of Eqn. (11) as

$$r_{n-1} Q_{n-1} \frac{i_{n-1}(t)}{Q_{n-1}} - (R_n + r_n) Q_n \frac{i_n(t)}{Q_n} = 0, \quad (33a)$$

$$r_{n-2} Q_{n-2} \frac{i_{n-2}(t)}{Q_{n-2}} - (R_{n-1} + r_{n-1}) Q_{n-1} \frac{i_{n-1}(t)}{Q_{n-1}} - R_{n-1} Q_n \frac{i_n(t)}{Q_n} = 0, \quad (33b)$$

⋮

$$r_1 Q_1 \frac{i_1(t)}{Q_1} - r_2 Q_2 \frac{i_2(t)}{Q_2} - R_2 \sum_{k=2}^n Q_k \frac{i_k(t)}{Q_k} = 0, \quad (33c)$$

The pack then behaves uniformly if the following generalised QR-condition is achieved

$$r_{n-1} Q_{n-1} = (R_n + r_n) Q_n \quad (34a)$$

$$r_{n-2} Q_{n-2} = (R_{n-1} + r_{n-1}) Q_{n-1} + R_{n-1} Q_n, \quad (34b)$$

⋮

$$r_1 Q_1 = (r_2 + R_2) Q_2 + R_2 \sum_{k=2}^n Q_k, \quad (34c)$$

as in,

$$r_j Q_j = r_{j+1} Q_{j+1} + R_{j+1} \sum_{k=j+1}^n Q_k. \quad (35)$$

When all cells have the same capacitances, as in $Q_j = Q_k$ for all j, k , then the condition for uniform branch currents in (35) simplifies to

$$r_j = r_{j+1} + R_{j+1} (n - j). \quad (36)$$

This condition shows that if the cells in packs with interconnection resistances are to receive the same current, then the series resistance of each cell should decrease at a rate proportional to the following interconnection resistance multiplied by its location relative to the back of the pack.

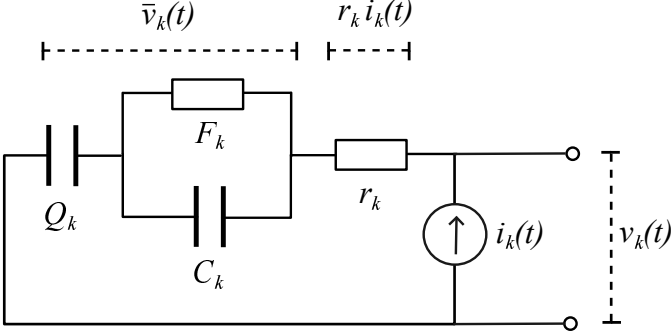


Fig. 5. Equivalent circuit model of the k^{th} cell in a parallel-connected pack.

TABLE I
CELL-LEVEL ECM PARAMETERS FOR MODEL VALIDATION USING
EXPERIMENTAL DATA FROM FOUR LG 21700 M50T CELLS CONNECTED IN
PARALLEL.

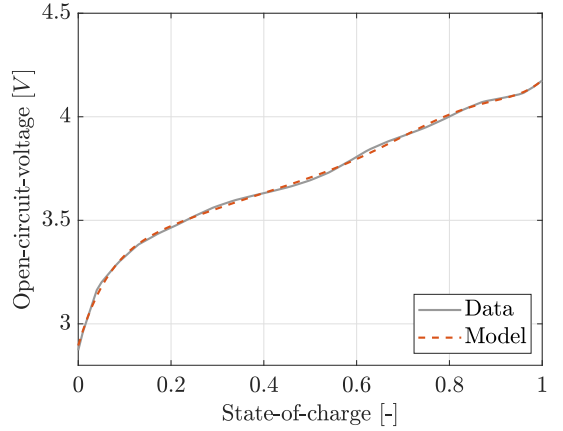
Parameter	Units
$r_k(z_k) = -0.056z_k^3 + 0.116z_k^2 - 0.073z_k + 0.0393$	[Ω]
$F_k(z_k) = -0.02248z_k^2 - 0.01228z_k + 0.02551$	[Ω]
$C_k = 2913.1$	[F]
$Q_k = 4.952$	[Ah]
$OCV(z_k) = 96.7822z_k^7 - 349.5041z_k^6 + 512.5251z_k^5$ $- 397.1122z_k^4 + 177.8325z_k^3 - 46.8445z_k^2$ $+ 7.6026z_k + 2.8955$	[V]

Designing the resistances of the pack to satisfy (36) could be achieved by adding additional shunt resistances along with the cells, with the number of added resistors increasing linearly towards the front of the pack. It is noted that [4] derived an equivalent condition for the case of two cells in parallel and provided experimental data to support the theoretical predictions; condition (36) basically extends that result to the case of n cells in parallel. Finally, it is noted that the expression (36) for uniform pack currents was achieved by working with the analytical solutions of Kirchhoff's laws explored in this paper; such expressions would be challenging to obtain with the numerical solutions.

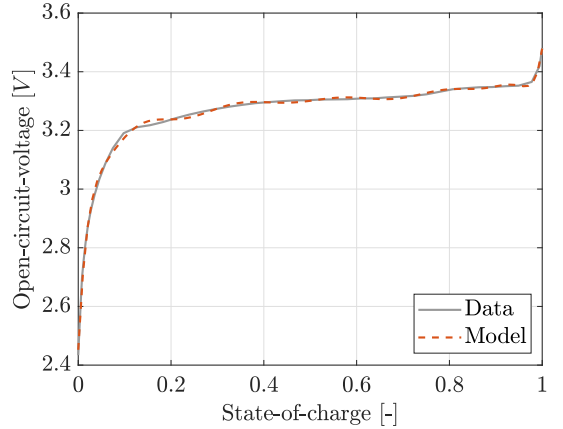
Figure 4 shows the impact of tuning the resistances across the pack following Eqn. (36). For the simulations, a pack of 10 LFP cells were connected in parallel using the parameters defined in Section V and charged at 1C. Figure 4a shows the evolution of the current distribution when each cell in the pack has the same resistance (as in $r_j = r_k$ for all $j, k = 1, 2, \dots, n$) whereas Figure 4b shows the flat current distribution obtained when the resistances satisfy (36). Exploring this notion further, Fig. 4c shows the increase in the initial current distribution across the pack as the ratio of the interconnection resistance, R_k , to series resistance, r_k , increases. In other words, as the interconnection resistance increases, the variation in the currents also increases as it becomes increasingly challenging for the currents to reach the cells at the back of the pack.

V. SIMULATION RESULTS AND DISCUSSION

In this section, the proposed modelling approach for parallel connected packs is analysed for two distinct Li-ion chemistries: NMC and LFP.



(a) SoC-OCV curve for LG 21700 M50T cells.



(b) SoC-OCV curve for K2 LFP26650P cells.

Fig. 6. Open-circuit voltage (OCV) curves used in the model simulations for different cell chemistries.

TABLE II
MSE BETWEEN SIMULATED AND MEASURED CELL CURRENTS FOR
 $R_k = 1 \text{ m}\Omega$ AND $R_k = 3 \text{ m}\Omega$.

R_k	Cell 1	Cell 2	Cell 3	Cell 4
1 $\text{m}\Omega$	0.0105	0.0032	0.0061	0.0298
3 $\text{m}\Omega$	0.0123	0.0187	0.0070	0.0141

A. Circuit model for the cells

For the model simulations, the cell-level dynamics of Eqn. (39) are described by the equivalent circuit models (ECM) of Fig. 5. For cells $k = 1, \dots, n$ (with n being the number of cells in parallel in the pack), this circuit maps the current $i_k(t)$ to the voltage $v_k(t)$ by

$$\frac{d}{dt} \begin{bmatrix} z_k(t) \\ w_k(t) \end{bmatrix} = \begin{bmatrix} 0 & 0 \\ 0 & -\frac{1}{F_k C_k} \end{bmatrix} \begin{bmatrix} z_k(t) \\ w_k(t) \end{bmatrix} + \begin{bmatrix} \frac{1}{Q_k} \\ \frac{1}{C_k} \end{bmatrix} i_k(t), \quad (37a)$$

$$v_k(t) = w_k(t) + \text{OCV}(z_k(t)) + r_k i_k(t), \quad (37b)$$

with $w_k(t)$ being the relaxation voltages caused by ion diffusion into active particles, $z_k(t)$ the state-of-charges (SoC) and $\text{OCV}(z_k(t))$ the open circuit voltages which are nonlinear functions of the SoC. The current going into cell k is denoted $i_k(t)$ and the voltage is $v_k(t)$. The voltage contribution from

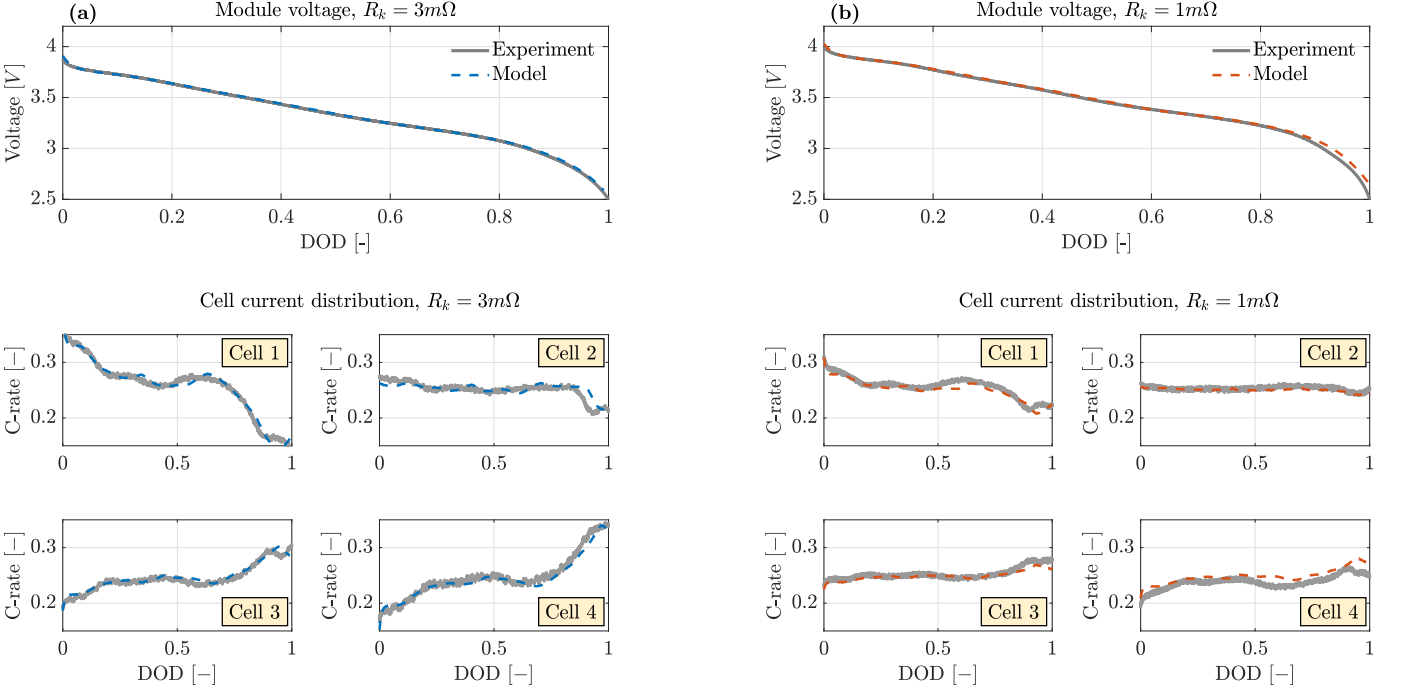


Fig. 7. Experimental validation of the parallel pack model using four *LG 21700 M50T* cells connected in parallel. Simulated and measured current and voltage profiles are shown for interconnection resistances of $R_k = 1 \text{ m}\Omega$ and $R_k = 3 \text{ m}\Omega$. DOD denotes the depth-of-discharge of the pack.

the state variables is

$$\bar{v}_k(t) = w_k(t) + \text{OCV}(z_k(t)). \quad (38)$$

In terms of parameters, $Q_k(t)$ is the cell's capacitance, F_k denotes the resistance of the RC-pair of the circuit model from Fig. 5 and $C_k(t)$ denotes its capacitance. It is recognised that the notation F_k for resistance is non-standard for ECMs but is adopted here since r_k was used for the series resistance and R_k for the interconnection resistance.

By defining cell k 's state as $x_k(t) = [z_k(t), w_k(t)]^\top$, the dynamics and voltage from Eqn. (37) can be represented as

$$\dot{x}_k(t) = \bar{A}_k x_k(t) + \bar{B}_k i_k(t), \quad k = 1, \dots, n, \quad (39a)$$

$$v_k(t) = \bar{v}_k(t) + r_k i_k(t). \quad (39b)$$

As such, the model is in the standard form of Eqn. (1) and so the solutions for the current distributions from Sections III-B and IV-C can be applied.

B. Experimental validation

The parallel-connected battery pack model was first validated against experimental data. Four *LG 21700 M50T* cells were connected in parallel with calibrated busbar interconnection resistances of 1 and 3 mΩ, both tested at 25°C. Details of the experimental procedures can be found in [40] and are not repeated here for the sake of brevity. The tested *LG 21700 M50T* cells were composed of LiNi_{0.8}Mn_{0.1}Co_{0.1}O₂ (NMC 811) cathodes and Graphite-SiO_x anodes and had capacitances of 4.85 Ah. The complete list of identified parameters for the cells is shown in Table I. The open-circuit voltage, OCV(z_k), of Table I was determined by fitting the experimentally measured values, as depicted in Figure 6a, with a polynomial

function of z_k . Following the approach of [41], the parameters of the dynamic components of the ECM (i.e., r_k , F_k , and C_k) were identified by minimizing the root mean square error between the model voltage and the measured cell voltage during time-varying Hybrid pulse power characterization (HPPC) current tests. To enhance model accuracy, r_k and F_k were also expressed as polynomial functions of z_k , as given in Table I. It is emphasised that this state-dependent characterisation of the resistance does not influence the solutions of Section III and IV—the only requirement is that the Ohmic drop is linear in the resistance.

Figure 7(a)-(b) compares the measured and simulated voltages for $R_k = 1$, and 3 mΩ, respectively, showing satisfactory model accuracy. The accuracy of the estimated cell current was assessed by computing the mean square error (MSE) between the model-estimated cell current and that measured by Hall sensors. The MSE values for each cell, in both module configurations, are reported in Table II. During a complete CC discharge cycle at a 0.75C rate, the error remained below 29.8 mA for all 8 cells tested. This corresponded to approximately 0.82% of the reference cell current at 0.75C (i.e., 0.75×4.85 Ah).

C. Parallel connected pack of LFP cells

With the parallel pack model validated against experimental data, further simulations were developed to analyse its behaviour. A pack of ten *K2 LFP26650P* cells with LFP cathodes and nominal capacitances of 2.6 Ah was considered for this analysis [42]. For $k = 1, 2, \dots, 10$, the capacitances were $C_k = 634 F$ and the resistances were modelled as Gaussian random variables, with $F_k \sim \mathcal{N}(0.0394, 0.001) \Omega$

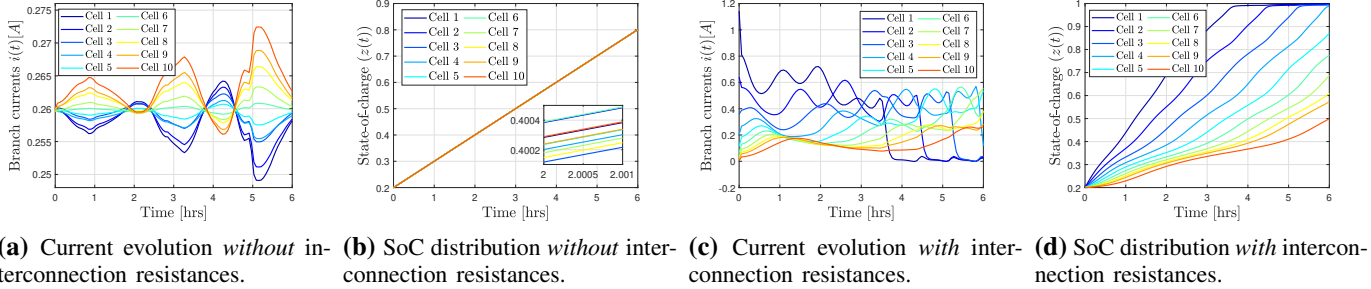


Fig. 8. Simulation results for a parallel-connected pack with LFP cells. Subfigures (a) and (b) correspond to the case without interconnection resistances, showing ideal branch currents and SoC distributions. Subfigures (c) and (d) show the impact of including interconnection resistances, where both branch currents and SoC deviate due to imbalance.

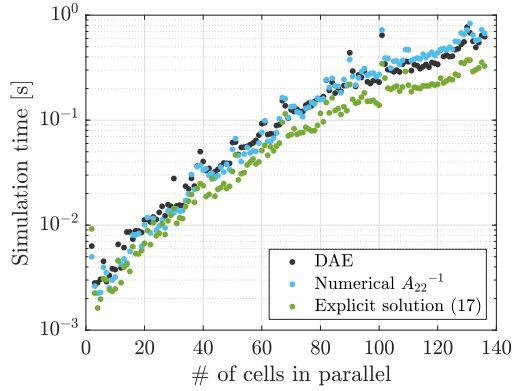


Fig. 9. Computation times for simulating LFP parallel connected packs models. A comparison between directly solving the DAEs and the formulation in terms of ODEs is shown. The DAEs and ODEs were solved using the MATLAB `ode15s` function.

and $r_k \sim \mathcal{N}(0.0291, 0.001) \Omega$. Experimental data of the SoC-OCV and its fit are shown in Fig. 6b [42].

The evolution of the branch currents without interconnection resistances is shown in Fig. 8a. The branch currents were relatively uniform, with each cell roughly charging at roughly the same rate (as shown in the SoC curves of 8b). However, when interconnection resistances were introduced, the current distribution became uneven, as depicted in Fig. 8c. As a result, the current imbalance caused by the interconnection resistances led to variations in the SoCs, as shown in Fig. 8d. These variations could lead to problems such as cell-to-cell variations in state-of-health, localised lithium plating, and thermal gradients in the pack. Recent experimental data such as [4] have demonstrated these cell-to-cell variations can appear in practice, with the current distributions generating inhomogeneous cell heating and, eventually, to the cells degrading at different rates [43]. By understanding how the different cells in the pack react through solutions such as Eqn. (25), improved mechanisms to reduce these pack-level heterogeneities could be designed.

Finally, Figure 9 shows the computational benefits of simulating parallel connected battery packs as ODEs rather than DAEs. The figure shows the growth in computation times for simulating LFP cells connected in parallel packs with $I(t) = 2$ C over 1080 s as the pack size increased from $n = 2$ to

$n = 135$. For these simulations, the standard deviation in the model parameters was reduced to 10^{-4} and $R_k = 10^{-5}$ to ensure the heterogeneities in the states of the large packs did not grow too large and cause additional numerical issues for the solvers. For each value of n , five simulations were run, and Figure 9 shows the average time of those five simulations. The DAE approach involved solving both Eqn. (1) and (11) using a “mass” matrix whereas the ODE approach either used the current distributions of Eqn. (17) or numerically inverted the A_{22} matrix of (13). Both the ODEs and DAEs were simulated using the MATLAB `ode15s` solver. In general, the simulations with the analytical solutions of (17) were faster than inverting the A_{22} matrix of (13) or directly solving the DAEs. These gains in simulation times accelerated as the pack size increased; at the end when $n = 135$, the ODE approach of Eqn. (17) took on average 0.355 s whereas the direct DAE approach with the mass matrix took 0.641 s. The accelerated simulation times indicate the analytical current distributions could enable cell-level modelling of the large packs now being deployed in the field, without resorting to lumped approximations.

CONCLUSIONS

This work introduces explicit solutions for the algebraic equations of Kirchhoff’s laws that characterise the current distributions across parallel connected lithium-ion battery packs. The solutions were expressed in terms of the pack models’ states, parameters, and the applied current and allows the model differential-algebraic-equations to be expressed explicitly in terms of ordinary differential equations. The main result was a solution for the current distribution across parallel connected packs with interconnection resistances—previously only numerical solutions that inverted matrices or applied approximate solutions were used. The results were validated against experimental data and in simulation for packs composed of both NMC and LFP cells and showed, amongst other features, the formation of current fluctuations and distributions across the pack. Compared to the experimental data, the model achieved an accuracy of 0.82% for the mean squared error of the branch currents, highlighting its effectiveness. These results could provide deeper insight into the complex dynamics of parallel connections, support pack design to reduce degrad-

tion heterogeneity, and enable pack-level battery management algorithms with robustness guarantees.

REFERENCES

- [1] J. T. Frith, M. J. Lacey, and U. Ulissi, "A non-academic perspective on the future of lithium-based batteries," *Nature Communications*, vol. 14, no. 1, p. 420, 2023.
- [2] J. M. Reniers and D. A. Howey, "Digital twin of a MWh-scale grid battery system for efficiency and degradation analysis," *Applied Energy*, vol. 336, p. 120774, 2023.
- [3] K. Vikrant, T. G. Tranter, G. M. Wiggins, D. J. Brett, and S. Allu, "Ageing studies of mega battery packs for grid storage applications using physics based modeling," in *Electrical Energy Storage Application and Technologies Conference (EESAT)*. IEEE, 2024, pp. 1–6.
- [4] K. Bhaskar, A. Kumar, J. Bunce, J. Pressman, N. Burkell, N. Miller, and C. D. Rahn, "Heterogeneity-induced power and capacity loss in parallel-connected cells," *IEEE Transactions on Transportation Electrification*, 2024.
- [5] M. Naylor Marlow, J. Chen, and B. Wu, "Degradation in parallel-connected lithium-ion battery packs under thermal gradients," *Communications Engineering*, vol. 3, no. 1, p. 2, 2024.
- [6] H. He, A. Fly, E. Barbour, and X. Chen, "Numerical investigation of module-level inhomogeneous ageing in lithium-ion batteries from temperature gradients and electrical connection topologies," *Communications Engineering*, vol. 3, no. 1, p. 89, 2024.
- [7] D. Zhang, L. D. Couto, R. Drummond, S. Sripad, and V. Viswanathan, "Cell-level state of charge estimation for battery packs under minimal sensing," *arXiv preprint arXiv:2109.08332*, 2021.
- [8] T. Rüwald, A. Marongiu, D. Chahardahcherik, H. van Faassen, H. Ditler, D. Schulte, and E. Figgemeier, "Experimental investigation of cell degradation in packs of parallel-connected cells under different temperature distributions," *Journal of Energy Storage*, vol. 104, p. 114427, 2024.
- [9] D. Zhang, L. D. Couto, S. Benjamin, W. Zeng, D. F. Coutinho, and S. J. Moura, "State of charge estimation of parallel connected battery cells via descriptor system theory," in *Procs. of the American Control Conference (ACC)*. IEEE, 2020, pp. 2207–2212.
- [10] J. A. Lone, N. K. Tomar, and S. Bhumik, "Functional observer design for parallel connected Li-ion battery: A descriptor systems theory approach," *IEEE Control Systems Letters*, vol. 7, pp. 961–966, 2022.
- [11] V. Sulzer, S. G. Marquis, R. Timms, M. Robinson, and S. J. Chapman, "Python battery mathematical modelling (PyBaMM)," *Journal of Open Research Software*, vol. 9, no. 1, 2021.
- [12] M. Torchio, L. Magni, R. B. Gopaluni, R. D. Braatz, and D. M. Raimondo, "Lionsimba: a Matlab framework based on a finite volume model suitable for Li-ion battery design, simulation, and control," *Journal of The Electrochemical Society*, vol. 163, no. 7, p. A1192, 2016.
- [13] Z. Khalik, M. Donkers, and H. J. Bergveld, "Model simplifications and their impact on computational complexity for an electrochemistry-based battery modeling toolbox," *Journal of Power Sources*, vol. 488, p. 229427, 2021.
- [14] M. D. Berliner, D. A. Cogswell, M. Z. Bazant, and R. D. Braatz, "Methods—PETLION: Open-source software for millisecond-scale porous electrode theory-based lithium-ion battery simulations," *Journal of The Electrochemical Society*, vol. 168, no. 9, p. 090504, 2021.
- [15] T. Tranter, R. Timms, V. Sulzer, F. Planella, G. Wiggins, S. Karra, P. Agarwal, S. Chopra, S. Allu, P. Shearing *et al.*, "Liionpack: A python package for simulating packs of batteries with PyBaMM," *Journal of Open Source Software*, vol. 7, no. 70, 2022.
- [16] M. Dubarry, A. Devie, and B. Y. Liaw, "Cell-balancing currents in parallel strings of a battery system," *Journal of Power Sources*, vol. 321, pp. 36–46, 2016.
- [17] T. Bruen and J. Marco, "Modelling and experimental evaluation of parallel connected lithium ion cells for an electric vehicle battery system," *Journal of Power Sources*, vol. 310, pp. 91–101, 2016.
- [18] E. Hosseinzadeh, J. Marco, and P. Jennings, "Combined electrical and electrochemical-thermal model of parallel connected large format pouch cells," *Journal of Energy Storage*, vol. 22, pp. 194–207, 2019.
- [19] L. Petzold, "Differential/algebraic equations are not ODE's," *SIAM Journal on Scientific and Statistical Computing*, vol. 3, no. 3, pp. 367–384, 1982.
- [20] G. Saccani, G. Ciaramella, and D. M. Raimondo, "A computationally efficient implementation of a battery pack electrochemical model using waveform relaxation," *Journal of Energy Storage*, vol. 46, p. 103758, 2022.
- [21] G. H. Golub and C. F. Van Loan, *Matrix computations*. JHU press, 2013.
- [22] A. Weng, H. Movahedi, C. Wong, J. B. Siegel, and A. Stefanopoulou, "Current imbalance in dissimilar parallel-connected batteries and the fate of degradation convergence," *J. Dyn. Syst. Meas. Control*, vol. 146, p. 011106, 2024.
- [23] R. Zhang, K. Wang, M. Chen, and G. Zhao, "Study of inhomogeneous performance for lithium-ion battery module in parallel connection," *Journal of The Electrochemical Society*, 2025.
- [24] J. P. Ross, E. Chatzinikolaou, D. F. Frost, S. R. Duncan, and D. A. Howey, "Comparison between battery cell level dynamics and pack level dynamics using equivalent circuit models," in *Procs. of the American Control Conference (ACC)*. IEEE, 2024, pp. 713–718.
- [25] T. K. Telmasre, L. Mishra, R. S. Thiagarajan, A. Subramaniam, V. Ramadesigan, T. R. Garrick, and V. R. Subramanian, "Initial current discrepancy in simulating lithium-ion battery packs-resolution from Dr. Ralph White's analytical approach," *Journal of The Electrochemical Society*, vol. 170, no. 10, p. 103512, 2023.
- [26] Y. Preger, J. Mueller, A. Fresquez, S. Allu, and C. Rich, "Impact of module configuration on lithium-ion battery performance and degradation: Part I. Energy throughput, voltage spread, and current distribution," *Journal of The Electrochemical Society*, vol. 172, no. 5, p. 050540, 2025.
- [27] S. M. Ayalasomayajula, Y. Preger, J. Mueller, and S. Allu, "Physics-based analysis of cell imbalances and aging in lithium-ion battery modules and packs," *Journal of The Electrochemical Society*, 2025.
- [28] R. Drummond, L. D. Couto, and D. Zhang, "Resolving Kirchhoff's laws for parallel Li-ion battery pack state-estimators," *IEEE Transactions on Control Systems Technology*, vol. 30, no. 5, pp. 2220–2227, 2021.
- [29] H. Lee, C. Casten, and H. K. Fathy, "State estimation for parallel-connected batteries via inverse dynamic modeling," *Journal of Energy Storage*, vol. 118, p. 116025, 2025.
- [30] A. Fill, S. Koch, A. Pott, and K.-P. Birke, "Current distribution of parallel-connected cells in dependence of cell resistance, capacity and number of parallel cells," *Journal of Power Sources*, vol. 407, pp. 147–152, 2018.
- [31] M. H. Hofmann, K. Czyrka, M. J. Brand, M. Steinhardt, A. Noel, F. B. Spangler, and A. Jossen, "Dynamics of current distribution within battery cells connected in parallel," *Journal of Energy Storage*, vol. 20, pp. 120–133, 2018.
- [32] G. Piombo, S. Fasolato, R. Heymer, M. Hidalgo, M. F. Niri, S. Onori, and J. Marco, "Unveiling the performance impact of module level features on parallel-connected lithium-ion cells via explainable machine learning techniques on a full factorial design of experiments," *Journal of Energy Storage*, vol. 84, p. 110783, 2024.
- [33] S. J. Moura, F. B. Argomedo, R. Klein, A. Mirtabatabaei, and M. Krstic, "Battery state estimation for a single particle model with electrolyte dynamics," *IEEE Transactions on Control Systems Technology*, vol. 25, no. 2, pp. 453–468, 2016.
- [34] S. Nejad, D. Gladwin, and D. Stone, "A systematic review of lumped-parameter equivalent circuit models for real-time estimation of lithium-ion battery states," *Journal of Power Sources*, vol. 316, pp. 183–196, 2016.
- [35] M. Doyle, T. F. Fuller, and J. Newman, "Modeling of galvanostatic charge and discharge of the lithium/polymer/insertion cell," *Journal of the Electrochemical society*, vol. 140, no. 6, p. 1526, 1993.
- [36] R. Drummond, A. M. Bizeray, D. A. Howey, and S. R. Duncan, "A feedback interpretation of the Doyle–Fuller–Newman lithium-ion battery model," *IEEE Transactions on Control Systems Technology*, vol. 28, no. 4, pp. 1284–1295, 2019.
- [37] R. Luca, M. Whiteley, T. Neville, T. Tranter, J. Weaving, J. Marco, P. R. Shearing, and D. J. Brett, "Current imbalance in parallel battery strings measured using a hall-effect sensor array," *Energy Technology*, vol. 9, no. 4, p. 2001014, 2021.
- [38] Z. Li, A. Zuo, Z. Mo, M. Lin, C. Wang, J. Zhang, M. H. Hofmann, and A. Jossen, "Demonstrating stability within parallel connection as a basis for building large-scale battery systems," *Cell Reports Physical Science*, vol. 3, no. 12, 2022.
- [39] P. Lambert, E. Tredenick, S. Duncan, and R. Drummond, "Detecting faulty lithium-ion cells in large-scale parallel battery packs using current distributions," 2023.
- [40] G. Piombo, S. Fasolato, R. Heymer, M. F. Hidalgo, M. F. Niri, D. M. Raimondo, J. Marco, and S. Onori, "Full factorial design of experiments dataset for parallel-connected lithium-ion cells imbalanced performance investigation," *Data in Brief*, vol. 53, p. 110227, 2024.
- [41] G. L. Plett, *Battery management systems, Volume II: Equivalent-circuit methods*. Artech House, 2015.

- [42] M.-K. Tran, A. DaCosta, A. Mevawalla, S. Panchal, and M. Fowler, "Comparative study of equivalent circuit models performance in four common lithium-ion batteries: LFP, NMC, LMO, NCA," *Batteries*, vol. 7, no. 3, p. 51, 2021.
- [43] W. Shi, X. Hu, C. Jin, J. Jiang, Y. Zhang, and T. Yip, "Effects of imbalanced currents on large-format LiFePO₄/graphite batteries systems connected in parallel," *Journal of Power Sources*, vol. 313, pp. 198–204, 2016.